THE ASTROPHYSICAL JOURNAL, 536:923–933, 2000 June 20

THE ATMOSPHERE OF MIRA VARIABLES: A VIEW WITH THE *HUBBLE SPACE TELESCOPE*

DONALD G. LUTTERMOSER[1,2,3]
Department of Physics, East Tennessee State University, Johnson City, TN 37614; lutter@etsu.edu
Received 1999 January 22; accepted 2000 January 31

ABSTRACT

Ultraviolet spectra obtained with *Hubble Space Telescope* (*HST*) of two Mira-type variable stars, R Leo and R Hya, are presented, along with analysis providing information on their outer atmospheres. These high-dispersion spectra were taken with the Goddard High Resolution Spectrograph (HRS) in two spectral regions: 2320–2368 Å to record the C II] (UV0.01) multiplet and 2785–2835 Å to obtain the Mg II *h* and *k* lines. The R Hya spectrum was obtained at visual light phase 0.26 and shows a Mg II spectrum that is very clean, showing clear evidence for the overlying circumstellar absorption from Fe I (UV3) and Mn I (UV1) over the *k* line. The fluoresced Fe I (UV44) feature at 2824 Å is plainly visible in this spectrum, whereas past *International Ultraviolet Explorer* (*IUE*) observations of Mira variables at high dispersion were unable to record this feature. Remarkably, the newly identified fluoresced Fe I (UV45) feature near 2807 Å is seen in this spectrum. Until now, this line has been seen only in cool carbon stars with *HST*/HRS. This line is pumped by the thin C II] (UV0.01) emission line at 2325.5 Å. Two of the strongest C II] (UV0.01) lines near 2325 Å are plainly seen in this spectrum. This region of the spectrum, however, is dominated by the Si II] (UV0.01) line near 2335 Å, in contrast to that observed in the carbon stars and the non-Mira oxygen-rich red giant stars. Very weak Mg II lines are seen in the R Leo spectrum at phase 0.12. At this phase, these lines are typically absent in *IUE* spectra. Velocity shifts of emission features in the UV spectra of Mira variables are consistent with previously published hydrodynamic models of these stars. These velocities indicate, however, that the C II] (UV0.01) emission lines are not formed in the same atmospheric layers as the Mg II emission. The electron density deduced from the C II] (UV0.01) multiplet is $\sim 10^9$ cm^{-3}. Finally, the temperature-density structure of the semiregular variable carbon stars is similar to the oxygen-rich Mira variables—both are hydrodynamic in nature; however, the carbon stars macroscopic velocity fields are not identical to the Mira stars in the atmosphere layers between the Mg II emission region and the circumstellar shell.

Subject headings: stars: abundances — stars: AGB and post-AGB — stars: variables: other (long-period variables) — ultraviolet: stars

1. INTRODUCTION

Detailed knowledge of the atmospheric structure of evolved giants stars is of fundamental importance, not only to the theory of stellar atmospheres, but to the understanding of stellar evolution and the chemical history of the Milky Way Galaxy. Mira-type variable stars are asymptotic giant branch (AGB) stars that show evidence for *somewhat* regular pulsations in their spectra and light curves. Emission lines seen in their spectra at visual wavelengths (e.g., Fe I lines and the hydrogen Balmer lines) vary in flux over the pulsation cycle (Bidelman & Herbig 1958; Wood 1975; Gillet 1988). Phase-dependent velocity measurements of these emission-line features indicate the presence of shock waves propagating through the outer envelopes of these stars (Willson 1976; Willson, Wallerstein, & Pilachowski 1982), which was first suggested by Merrill (1940). The *International Ultraviolet Explorer* (*IUE*) spacecraft has shown that ultraviolet (UV) emission-line variability also is correlated with pulsations (Brugel et al. 1987; Bookbinder, Brugel, & Brown 1989; Luttermoser 1996). In addition to the more typical collisionally excited lines, Mira variables also show strong fluorescent lines at both visual and UV wavelengths (Bidelman & Herbig 1958; Luttermoser 1996). Fe I (42) at 4202 and 4308 Å, both pumped by the Mg II *k* line, are a good example of this fluorescence.

In an attempt to understand the brightness variability and spectra, astronomers have been modeling the atmospheres of these stars with a variety of techniques. Sophisticated hydrodynamic models have been generated for these stars (e.g., Drinkwater & Wood 1985; Bowen 1988; Fleischer, Gauger, & Sedlmayr 1992; Bessell, Scholz, & Wood 1996; Hoefner & Dorfi 1997). Luttermoser & Bowen (1990, 1992) and D. G. Luttermoser, G. H. Bowen, & L. A. Willson (1999, in preparation) have used the Bowen (1988) models to generate non-LTE synthetic spectra.

The *IUE* archives contain an enormous amount of data concerning Mira variables. However, *IUE* did not have the sensitivity to reach the faint C II] (UV0.01) intersystem multiplet near 2325 Å under high dispersion. This multiplet is sensitive to the electron density of the gas emitting these photons (e.g., Stencel et al. 1981; Lennon et al. 1985). As such, we have used the Goddard High-Resolution Spectrograph (HRS) on the *Hubble Space Telescope* (*HST*) to record these features in two Mira-type variable stars, R Leo and R Hya, along with the Mg II features near 2800 Å. This data will be a strong constraint to the atmospheric models that are now being generated for these types of stars.

We discuss the spectral observations and the data reduction in § 2. A detailed analysis of this data is presented in § 3 along with its implications concerning the kinematic

[1] Member of the Institute for Mathematical and Physical Sciences, East Tennessee State University.

[2] Guest Observer with the *Hubble Space Telescope* and the *International Ultraviolet Explorer*, both operated by the National Aeronautics and Space Administration.

[3] Visiting Astronomer, Kitt Peak National Observatory and National Solar Observatory, NOAO, operated by the Association of Universities for Research in Astronomy, Inc. (AURA), under cooperative agreement with the National Science Foundation.

properties (flows, turbulence) of the outer atmospheres. In § 4, a discussion of the results learned from the spectra and comparisons to other types of red giant stars are made. Finally, concluding remarks about this work are presented in § 5.

2. OBSERVATIONS

Mira variable stars typically change in brightness at visual wavelengths of at least 2.5 mag with periods greater than 150 days. They are predominantly M-type stars, but smaller percentages exist for the S and C spectral classes. Two basic types of emission lines exist in the spectra of Mira stars: *collisionally excited lines* [e.g., Mg II *h* and *k*, Fe II [UV1, UV62, UV63], H Balmer lines] and *fluoresced lines* [e.g., Fe I (42) at 4202 and 4308 Å]. Fluoresced lines are pumped by photons from an emission line at a different wavelength from the fluoresced line [e.g., in the case of the Fe I (42) lines, Fe I (UV3) at 2795.006 Å absorb emission-line photons from the Mg II *k* line at 2795.523 Å, electrons then cascade back down a different transition, thus giving rise to the Fe I (42) features]. One problem that has existed prior to *HST* was the inability of *IUE* to record the C II] (UV0.01) multiplet near 2325 Å. These lines are important since flux ratios of various lines in this multiplet give an accurate measure of electron density in the region of the atmosphere giving rise to these lines (Stencel et al. 1981; Lennon et al. 1985). With the greater light-gathering power of *HST*, these weak features can now be recorded at high dispersion.

Comparisons will be made between velocity shifts of line profiles and the center-of-mass (i.e., radial) velocity of the stars in our sample. This velocity is not easy to derive in Mira variables, since absorption lines in these stars often exhibit variable Doppler shifts because of the dynamic nature of their atmospheres (e.g., Barnbaum 1992; Hinkle, Lebzelter, & Scharlach 1997; Udry et al. 1998). Currently, the best estimate for the center-of-mass velocity is provided by the CO microwave rotational lines, which forms high above the photosphere. Hinkle et al. (1997) cite -11.8 km s^{-1} for the center-of-mass velocity of R Hya. Note, however, that Zuckerman & Dyke (1986) measured a value of -9.9 km s^{-1} for this velocity based on measurements of the CO (2–1) emission, Loup et al. (1993) cites a value of -10 km s^{-1} based on CO (1–0), and Young (1995) gives a radial velocity of -10.0 ± 0.2 for R Hya based upon CO (3–2) and (4–3) lines. For this work, we will use -10.0 km s^{-1} as the center-of-mass velocity of R Hya. Hinkle, Scharlach, & Hall (1984) give an average of $+7.2 \pm 1.0$ km s^{-1} for R Leo based upon both CO and SiO rotational lines. Later, comparisons will be made to a sample of non-Mira red giants; two semiregular-variable carbon stars, UU Aur (N3 II; C6,4) and TX Psc (N0 II; C6,2), and the oxygen-rich red giant μ Gem (M3 III). The center-of-mass velocities used for these stars are $+6.8$ km s^{-1} for UU Aur, $+12.2$ for TX Psc (both from CO data of Olofsson et al. 1993) and $+54.8$ km s^{-1} for μ Gem (Wilson 1953).

2.1. *HST*/HRS Spectra

Prior to the *HST* servicing mission under GO Program 6620, we were able to obtain data of two different (but similar) Mira variables at two different phases: R Hya, at phase 0.26, taken on 1996 July 9 with the G270M grating through the large science aperture (LSA), and R Leo, at phase 0.12, taken on 1997 January 14 with the same telescope configuration (see Table 1). In order to compensate for thermal drifts in the HRS, SPYBAL observations were made between the longer exposures of the targets. Also note that COSTAR was deployed for each of the observations. The Mg II observations for both stars were taken with FP-SPLIT = 4 to minimize effects of the response irregularities in the photocathode detectors. Meanwhile, because of the expected low flux levels of the spectra in the C II] regime, FP-SPLIT was turned off; however the long exposures were split into two separate exposures to help reduce any long-term wavelength shifts caused by thermal changes in the detectors (see Table 1). Note that the recommended maximum exposure length of five to ten minutes could not be followed because of the expected extreme low fluxes of the C II] lines.

These observations were concerned primarily with obtaining accurate fluxes of the Mg II and C II] (UV0.01) emission features in the spectra. Exact shapes and velocities of the line profiles were of secondary importance. Hence, the LSA was used along with standard wavelength calibrations during this observing program. Data was retrieved from the magnetic tapes using the STSDAS "strfits" procedure under IRAF. Final reduction of the data was made using the STSDAS procedures "poffsets," "specalign," and "mkmultispec" following the directions detailed in the

TABLE 1

Hubble Space Telescope HRS Spectra and SPYBAL Frames for R Leo and R Hya

Observation Identification	Grating	Aperture	Observation Date and Time (UT)	λ (Å)	Exposure Time (s)
R Leo (HD 84748)					
Z3C90303T	G270M	SC2	1997 Jan 14 11:04	2878.6–2923.9	4.8
Z3C90304T	G270M	LSA	1997 Jan 14 11:05	2786.6–2833.8	1583.8
Z3C90305T	G270M	LSA	1997 Jan 14 12:30	2321.1–2368.9	2720.0
Z3C90306T	G270M	SC2	1997 Jan 14 14:07	2878.7–2924.0	4.8
Z3C90307T	G270M	LSA	1997 Jan 14 14:08	2321.1–2368.9	5440.0
R Hya (HD 117287)					
Z3C90103T	G270M	SC2	1996 Jul 9 05:30	2878.6–2923.9	4.8
Z3C90104T	G270M	LSA	1996 Jul 9 05:32	2786.3–2833.4	1088.0
Z3C90105T	G270M	LSA	1996 Jul 9 05:53	2320.8–2368.6	3264.0
Z3C90106T	G270M	SC2	1996 Jul 9 08:29	2878.6–2923.9	4.8
Z3C90107M	G270M	LSA	1996 Jul 9 08:30	2320.8–2368.6	5440.0

HST Data Handbook (Leitherer 1995). Data analysis was handled using the *Interactive Data Language* (IDL) with procedures written by the author. Before performing this analysis, ASCII files were made of the reduced data using the STSDAS procedure "imtab."

Flux, wavelength, and header information were stored in one ASCII file from the files generated above using IDL. With the help of Carpenter, Robinson, & Judge (1995) and the *Ultraviolet Multiplet Tables* (Moore 1950), line identifications were made for both emission and absorption features, and FWHM and line shifts were determined for the emission features, once again, using IDL procedures written by the author. The absolute throughput of the LSA is poorly known; however it is estimated that the flux uncertainly of stellar objects taken through the LSA with COSTAR is between 5% and 10% of the observed flux. The wavelength uncertainties are approximately 0.03 Å (3.6 km s^{-1}) in all spectra and the spectral resolution is 0.13 Å ($\sim$14 km s^{-1}) in both the C II] and Mg II regions.

2.2. *IUE Observations*

For comparison purposes, a sample of high-dispersion *IUE* spectra are displayed for a variety of phases for R Leo. These observations were obtained for an observing campaign that monitored both Mira-type red giant variable stars and semiregular variable stars at both UV and visual wavelengths in order to investigate the fluorescent lines that are often seen in the blue spectral regions of Mira variables (see D. G. Luttermoser, 1999, in preparation). These spectra were obtained during the fourteenth year of *IUE* mission under program LGNDL and the fifteenth year under program CVODL (see Table 2). Each spectrum was taken through the large aperture of *IUE* with the LWP camera. These spectra were reduced using the standard *IUE* RDAF IDL procedures. For days where multiple high-dispersion exposures were made of R Leo, the spectra were coadded to improve the signal-to-noise ratio. Saturated pixels and radiation hits were not included in the coadded spectra. The spectral resolution of these spectra are 0.15 Å ($\sim$16 km s^{-1}) at Mg II.

2.3. *McMath-Pierce Stellar CCD Observations*

The above mentioned monitoring program also included a series of ground-based observations taken with the National Solar Observatory (NSO) Stellar CCD Spectrograph on the McMath-Pierce Telescope on Kitt Peak, Arizona. Two observations from this program are presented here: (1) a 60 minute exposure taken on 1994 May 16 at 5:16 UT in the wavelength regime 4176–4279 Å, and (2) a 35 minute exposure taken on 1994 May 16 at 3:47 UT in the 4280–4381 Å regime. The spectral resolution of these spectra were 0.20 and 0.22 Å, respectively, and the respective wavelength errors were 0.0039 and 0.0057 Å as deduced from the wavelength calibration. These observations were obtained under the NSO Synoptic Observing Program (ID: 1545) using the 105 mm transfer lens, five-element image slicer, and the Milton & Roy Blue Grating. Guiding was carried out on the target star by use of a dichroic filter at the entrance aperture of the slicer, which fed the *red* light from the star to the guider television camera. The data reduction was carried out using IDL procedures written by the author. The details of these reductions can be found in D. G. Luttermoser (1999, in preparation).

3. SPECTRAL ANALYSIS

At visual wavelengths, the strongest emission lines seen are the hydrogen Balmer lines. The peak Balmer line flux occurs at phase 0 (which is defined to be the maximum visual brightness). Typically, around phase 0.2, emission lines from neutral metals, particularly Fe I, begin to appear in the blue and these reach a peak flux around phase 0.3–0.4 as the star pulsates.

At UV wavelengths (as observed with *IUE*), emission lines do not appear until phase 0.15, at which point they continue to gain strength in time until reaching a maximum around phase 0.3–0.4, similar to the neutral metal lines. Figure 1 shows a series of high-dispersion *IUE* spectra of R Leo in the Mg II *h* and *k* region. Most non-Mira red giant stars display *effectively thin* Mg II *h* and *k* lines (e.g., Judge et al. 1993)—lines that show double-lobed emission features with an integrated flux ratio of $F(k)/F(h) \approx 1.5$, the ratio of their respective oscillator strengths. *IUE* observations have shown us that this is not the case for Mira variable stars. When Mg II is near its peak flux ($\sim$ phase 0.3–0.4), $F(k) < F(h)$, then slowly take on the more normal, effectively thin $F(k)/F(h) > 1$ as the flux of these lines fade past phase 0.5 (D. G. Luttermoser, 1999, in preparation). These *IUE* spectra give a strong indication that the relative weak-

TABLE 2

IUE SPECTRA FOR R LEO

Camera Identification	Observation Date and Time (UT)	Exposure Time (minutes)	Phase	Notes
		Program LGNDL		
LWP22707	1992 Mar 29 17:50	120.0	0.49	
LWP22708	1992 Mar 29 20:16	90.0	0.49	Mg II *k* slightly overexposed
LWP22894	1992 Apr 26 14:41	150.0	0.59	Mg II *k* 2 times overexposed
LWP22895	1992 Apr 26 17:27	90.0	0.59	
LWP22896	1992 Apr 26 19:36	80.0	0.59	
		Program CVODL		
LWP24293	1992 Nov 7 20:28	90.0	0.21	
LWP24684	1993 Jan 8 16:05	60.0	0.40	
LWP24688	1993 Jan 8 21:52	60.0	0.40	
LWP25280	1993 Apr 6 16:55	180.0	0.70	
LWP25431	1993 Apr 28 14:26	180.0	0.27	

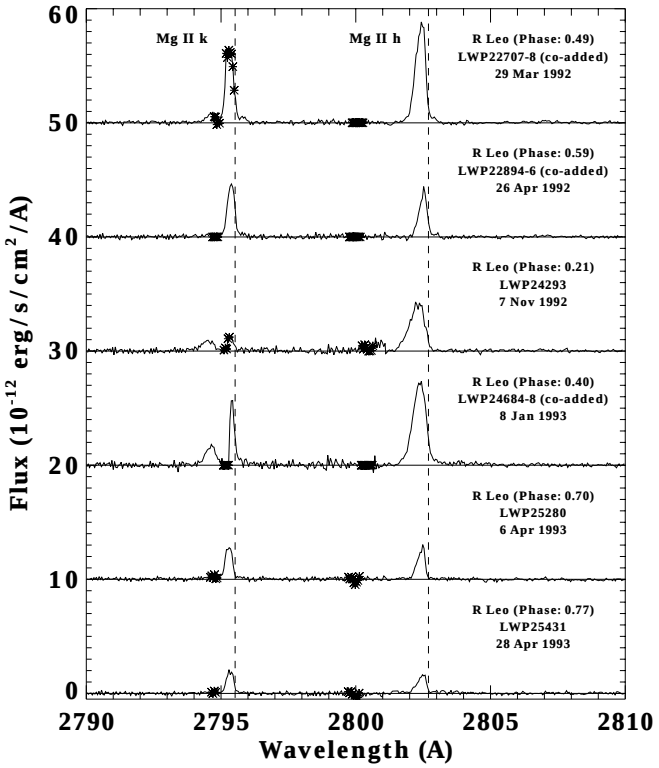

FIG. 1.—Series of high-dispersion *IUE* spectra of R Leo in the Mg II *k* and *h* region taken at various phases over two pulsation cycles. Reseau marks and saturated pixels are marked with asterisks. All spectra have been shifted by -7.2 km s^{-1} to offset the center-of-mass velocity of R Leo (see text). Laboratory wavelengths of Mg II *h* and *k* are indicated with a vertical dashed line.

ness of the *k* line with respect to the *h* line results from absorption from Fe I and Mn I in a cooler overlying shell. Another obvious feature of the Mg II doublet is the large blueshift of the emission of these lines with respect to the rest velocity of the star (as shown by *dashed lines* in Fig. 1). Such blueshifts are not seen in the non-Mira red giants and the cause of this shift is still debated (see D. G. Luttermoser, 1999, in preparation, for further analysis of this *IUE* data).

Higher spectral resolution of the Mg II lines is required to ascertain securely the identity of the overlying absorption features and to improve the understanding of the physics in the outer atmospheres in Mira variables. As such, the previously mentioned *HST*/HRS observations were obtained to address the problem. Figure 2 shows the Mg II lines in the spectrum of R Leo at phase 0.12—the lines are just starting to rise out of the noise. This *HST*/HRS spectrum is the earliest (in phase space) these lines have been seen in a Mira. Note that the flux of the *k* line is approximately twice as great as the *h*, similar to that seen in warmer red giant stars. Later, as these lines strengthen, *h* becomes stronger than *k* because of the interaction of the *k* line photons with the overlying circumstellar absorption lines. However, the C II] (UV0.01) lines are still too faint to be seen at this phase.

Figure 3 shows Mg II at phase 0.26 in R Hya. As was seen with *IUE*, the Mg II *h* and *k* lines are blueshifted with respect to the stellar rest frame (*dashed lines*). The fluoresced Fe I (UV45) line (pumped from C II] λ2325.4) is also blueshifted whereas the Fe I (UV44) line (pumped from Mg II *k*) is relatively stationary with respect to the star. Meanwhile, Figure 4 shows the C II] (UV0.01) lines at this same phase

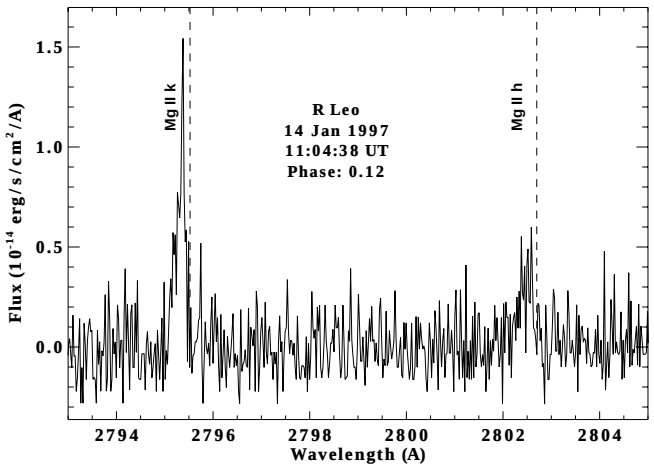

FIG. 2.—R Leo at phase 0.12 on 1997 January 14 in the Mg II *h* and *k* region taken with the *HST*/HRS. Observed spectrum has been shifted by -7.2 km s^{-1} to the stellar rest frame.

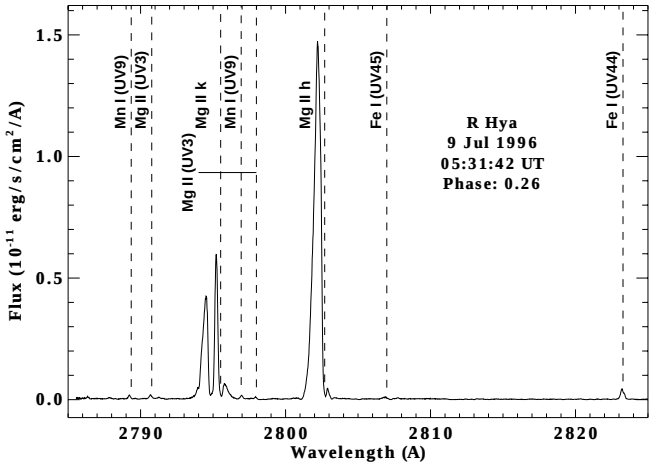

FIG. 3.—R Hya in the Mg II region at phase 0.26 on 1996 July 9 as recorded by *HST*/HRS. All emission features are identified. A wavelength shift of $+10$ km s^{-1} has been made to present the data in the stellar rest frame.

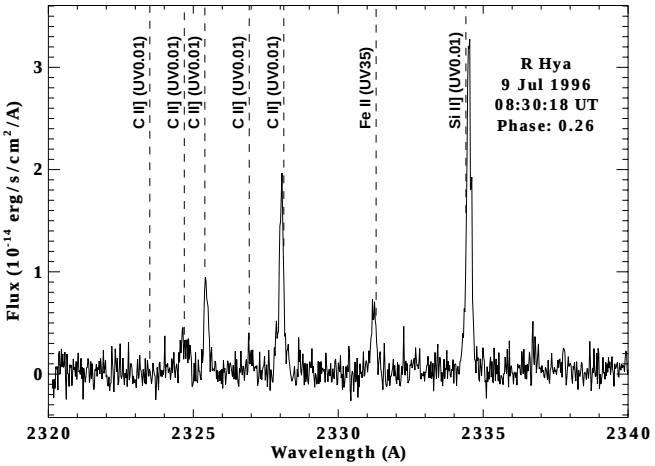

FIG. 4.—R Hya in the 2330 Å region at phase 0.26 on 1996 July 9. This spectrum has been shifted by $+10$ km s^{-1} to the stellar rest frame.

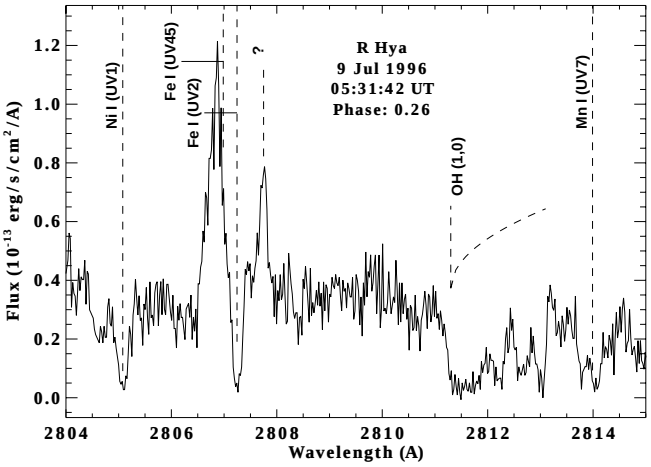

FIG. 5.—As was first noted in the *HST*/HRS spectra of cool carbon stars, oxygen-rich Mira stars also show the fluoresced Fe I (UV45) emission line at 2807.0 Å, which is *pumped* by C II]. Prominent absorption features also are identified.

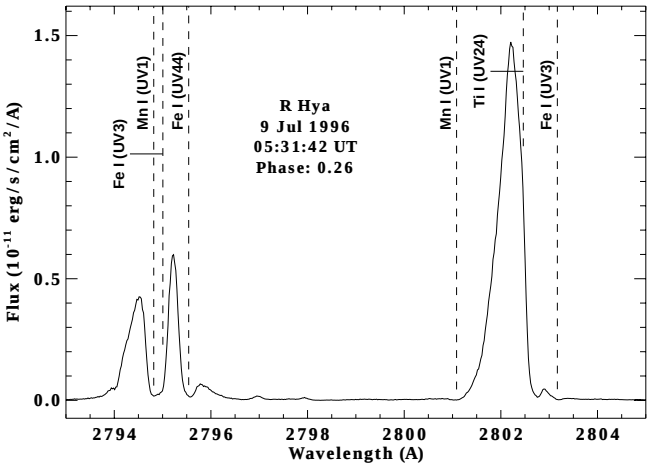

FIG. 6.—Location of strong circumstellar absorbers in the vicinity of Mg II.

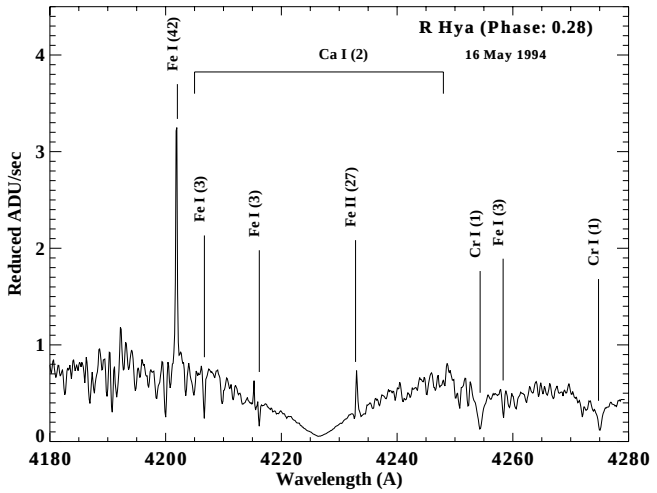

FIG. 7.—Strong fluoresced Fe I (42) line near 4202 Å obtains its greatest flux at the same epoch in phase space as the Mg II *h* and *k* lines in Mira variables. Observations taken with the McMath-Pierce telescope at KPNO.

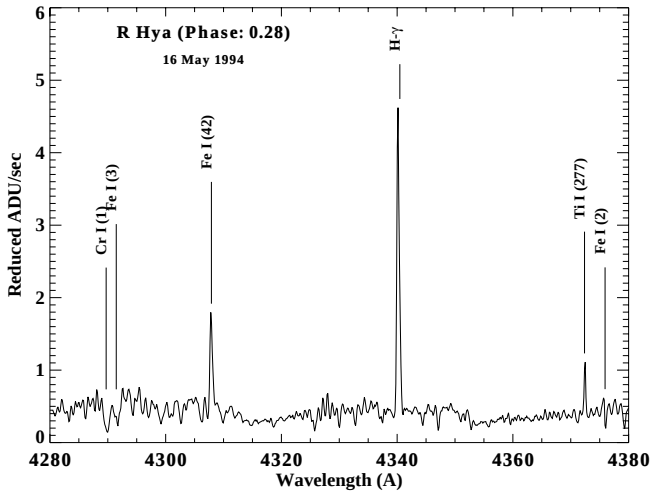

FIG. 8.—Collisionally excited (Hγ) and fluoresced [Fe I (42) and Ti I (277)] lines of Mira variables at visual wavelengths. Spectrum obtained with the McMath-Pierce telescope at KPNO.

for R Hya. This is the *first* time the C II] (UV0.01) multiplet has been recorded in a Mira variable under high dispersion. The flux ratio of lines in this multiplet can be used to measure electron density. Unfortunately, the usually strong line at 2325.4 Å is compromised by circumstellar absorption from an Fe I (UV13) transition at 2325.3 Å. The weak flux of the lines at 2324.7 and 2326.9 Å suggests an electron density of $\sim 10^9$ cm^{-3}; however, the uncertainties are large ($\sim 30\%$) because of the noise.

With the help of Carpenter, Wing, & Stencel (1985), we have identified some of the absorption features seen in the UV spectra of Mira variables. One of the most obvious absorption features in Figure 5 is the OH (1, 0) R_1 bandhead near 2811 Å.

One surprising feature has been seen in the spectrum of R Hya—the Fe I (UV45) emission line at 2806.984 Å (Fig. 5). This fluoresced line was first discovered in the *HST*/HRS spectrum of the carbon star UU Aur (Johnson et al. 1995) and is *pumped* by the thin C II] line at 2325.398 Å through an Fe I (UV13) transition at 2325.320 Å (see Luttermoser 1999 for a description of the discovery of this mechanism). This is the first time this fluoresced-emission feature has been seen in a noncarbon star! The appearance of this feature in oxygen-rich stars suggests that one need only an appreciable circumstellar shell over a *chromosphere* (i.e., an enhanced temperature regime in the outer atmosphere) to produce this feature. Unfortunately, this fact prevents us from using this line to determine the electron density in these stars. Deeper observations with the Space Telescope Imaging System (STIS) will be required to retrieve this information from the fainter, *noncompromised* C II] lines at 2324.689 and 2326.930 Å.

The emission feature just longward of the strong Fe I (UV2) absorption line has proven to be quite a challenge to identify. A search of the *Ultraviolet Multiplet Tables* (Moore 1950) gives four possible identifications of this feature: Y I (UV2) at 2807.66 Å (giving a emission-line velocity shift of $+9.5$ km s^{-1} with respect to the center-of-mass velocity); Mo II (UV5) at 2807.750 Å (-0.1 km s^{-1}), Tc II (UV4) at 2807.915 Å (-17.7 km s^{-1}), and Mn I (UV6) at 2808.015 Å (-28.4 km s^{-1}). It should be noted here that the uncertainties in the velocity measurements of the emis-

sion lines in this spectrum are much less than the uncertainty in the center-of-mass velocity as noted at the beginning of § 2. The majority of the UV emission lines seen in this star are blueshifted with respect to the center-of-mass velocity, so Mn I (UV6) is an unlikely candidate even though the Mn I (UV9) multiplet is seen in emission. Also, no other Mn I (UV6) multiplet lines are seen in emission. Likewise, it is unlikely that this λ2807.749 emission line is caused by Mo II (UV5) since no other lines from this multiplet are seen in emission in this spectrum. Of the three lines in the Y I (UV2) multiplet, two are near emission features: the line in question and the 2791.20 Å line. If the observed emission feature near 2791.2 Å is due to this transition, it is shifted by $+7.1$ km s^{-1}, similar to the 2807.66 Å line. However, both of these transitions are much weaker than the transition at 2813.64 Å, and no emission feature is seen near this wavelength. As such, it is unlikely that the emission line at 2807.749 Å is caused by Y I (UV2). Neutral technetium has been detected in this star at visible wavelengths (Little, Little-Marenin, & Bauer 1987). Like the previous possibilities, no other transition in the Tc II (UV4) multiplet are seen in emission. However, one of the lines in this multiplet (a^5G–z^5G°) resides at 2795.778 Å and is coincident with the broad emission of the Mg II *k* line. Unfortunately, this coincident Tc II (UV4) transition has an upper-level *J*-value of 6 whereas the 2807.915 Å line has $J = 5$ for its upper energy level; as such, singly ionized technetium fluorescence is not the cause of this emission feature. A search of other Tc II (UV4) lines with an upper level of $J = 5$ shows no coincidences with strong emission features. The Tc II (UV4) transition that is coincident with the Mg II *k* emission does share the same upper level with a transition at 2797.730 Å and an emission line is seen close to this wavelength. However, Mg II (UV3) lies at 2797.989 Å and is the cause of this emission feature [i.e., Mg II (UV3) at 2790.768 Å also is seen]. As such, this mysterious feature at 2807.75 Å is not Tc II. Since Moore's *Multiplet Tables* are not complete, the National Institute of Standards and Technology Web pages were accessed (http://physics.nist.gov/PhysRefData/ASD1/choice.html) and all transitions in their database within 0.3 Å of 2807.75 Å sought. An additional possible transition near this wavelength was found, Sc II (UV4). Unfortunately, no other lines in this multiplet are seen and with a lower energy level of 3.4 eV, it is unlikely that Sc II is the source of this emission feature. As such, the emission feature at 2807.75 Å will remain unidentified.

The Mg II *h* and *k* lines are one of the main driving forces behind the various fluorescent features that are seen at visual wavelengths of Mira variables. Figure 6 shows the stellar rest-frame position of neutral-metal lines that absorb Mg II photons, which are then reemitted at visual wavelengths (see Figs. 7 and 8). Overlying absorption from a circumstellar shell (i.e., the extreme outer atmosphere of the star) severely mutilates the Mg II resonance lines. In Mira stars, absorption from circumstellar Fe I (UV3) gives rise to the strong fluorescent lines of Fe I (42) at 4202 and 4308 Å as shown in Figures 7 and 8. The Mn I (UV1) resonance line at 2794.817 Å also produces fluoresced lines at visual wavelengths (Bidelman & Herbig 1958). A new fluoresced line at 4372.4 Å caused by Ti I (277) is identified and its pump is identified here as Ti I (UV24) at 2802.465 Å, which absorbs Mg II *h*-line photons. This Ti I (277) feature mimics the same flux-variation pattern as the Fe I (42) lines, which further supports the Mg II *h*-line pump scenario.

4. DISCUSSION

It is interesting to note the differences and similarities in the UV emission lines for the various spectral and variability classes of red giant stars. Figures 9 and 10 show such comparisons. R Hya is an M7 Mira variable with an effective temperature of 2680 $\pm$ 70 K when at phase 0.28 (Haniff, Scholz, & Tuthill 1995), which is close to the phase at which the HRS observations were made. For comparison, HRS spectra are displayed for μ Gem, a nonvariable M3 red giant with an effective temperature of 3587 $\pm$ 93 K (Di Benedetto & Conti 1983), TX Psc, a carbon star with an effective temperature of 3090 $\pm$ 125 K (Jørgensen 1989; Quirrenbach et al. 1994), and UU Aur, a cooler carbon star at an effective temperature of 2767 $\pm$ 25 K (Quirrenbach et al. 1994). Both of the carbon stars are semiregular (i.e., non-Mira) variable stars. In Mira stars, the Mg II line emission is shifted blueward of the stellar rest velocity, whereas the semiregular, oxygen-rich variable stars and the nonvariable red giants display Mg II emission, which is virtually at rest with respect to the stellar photosphere of the star. Also note that circumstellar absorption is not evident in the earlier red giant star μ Gem [i.e., $F(k)/F(h) \approx 1.5$]—only the narrow interstellar absorption is seen blue shifted from the self-absorption of the upper stellar atmosphere. Indeed, in terms of UV spectra, the carbon-rich (non-Mira) giants appear more similar to the oxygen-rich Mira variables—Mg II *k* and *h* mutilation by overlying absorption and the appearance of the fluoresced Fe I (UV45) emission line in both spectra.

Meanwhile, the flux ratio of various lines in the optically thin C II] (UV0.01) multiplet (e.g., λ2325.40/λ2328.12, λ2325.40/λ2326.93, and λ2324.69/λ2326.93—Lennon et al. 1985) indicate the electron density of the gas that gives rise

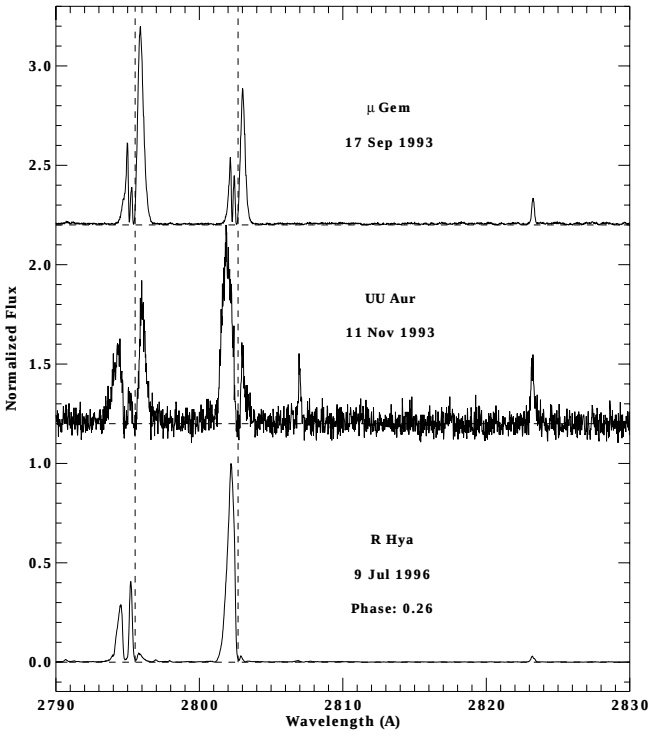

FIG. 9.—Three comparison *HST*/HRS spectra in the Mg II spectral region. Each spectrum has been shifted to the rest frame of the star in question and their peak fluxes have been normalized to unity. Vertical dashed lines represent the laboratory wavelengths of Mg II *h* and *k*.

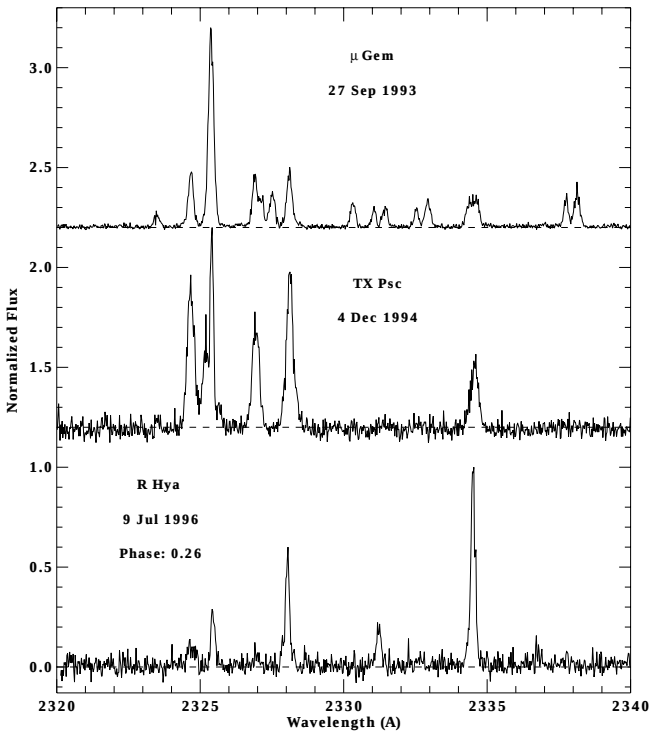

FIG. 10.—C II] and Si II] lines for oxygen-rich and carbon-rich red giant stars. Note the overlying absorption on the C II] line at 2325.5 Å from Fe I (UV13) at 2325.3 Å. It is this absorption that gives rise to the Fe I (UV45) emission line at 2807.0 Å in both the carbon stars and the Mira stars. Each spectrum has been shifted to the rest frame of the star in question and their peak fluxes have been normalized to unity.

to the emission. In Figure 10, one can plainly see a clear difference in the overall appearance of the C II] multiplet in the oxygen-rich, non-Mira (μ Gem), the carbon-rich, non-Mira (TX Psc), and the oxygen-rich, Mira (R Hya). Carpenter et al. (1997) found an electron density of 10^9 cm^{-3} for TX Psc using the λ2324.69/λ2326.93 ratio but noted that this value is uncertain because of the possibility that the C II] multiplet may not be optically thin in this star. However, the μ Gem C II] spectrum implies an electron density of 3×10^8 cm^{-3} at the depth of formation of these ionized carbon lines. Although the uncertainties are high, the electron density in both TX Psc and R Hya are a factor of 3 greater than that of the nonvariable M-star μ Gem. These higher electron densities may be an observational characteristic of red giant stars with shocked atmospheres.

Tables 3 and 4 list the five stars in our sample and tabulate the integrated flux the Mg II resonance lines and the C II] (UV0.01) multiplet, normalized by the K-magnitude flux (Table 3), and the velocity information of the C II] lines and the UV fluoresced lines [e.g., Fe I (UV44) at 2823.3 Å and Fe I (UV45) at 2807.0 Å—Table 4]. Note the ratio of the integrated flux between the Mg II k and the Mg II h lines. The k line should be approximately twice as strong as the h line for these *effectively thin* lines. Circumstellar absorption from neutral metal lines is the cause of this ratio being less than unity and the identification of these features can be made securely from the R Hya spectrum. Strangely, the circumstellar absorption at earlier phases in a Mira variable star's cycle is not apparent (e.g., R Leo at phase 0.12). This can be understood by noting the FWHM of the Mg II features—these lines simply are not wide enough at early phases to interact with the Fe I (UV3) or Mn I (UV1) multiplet lines.

Another interesting observation concerns the Fe I (UV45) fluorescence. Twenty percent of the C II] flux goes into pumping this feature in the carbon star. However, 6 times the amount of flux seen in the C II] lines comes out in this Fe I line in the Mira star! There are numerous differences between the atmospheric structure of oxygen-rich versus carbon-rich stars and Mira versus non-Mira red giant variables (Johnson 1987; Judge 1989; Judge & Stencel 1991; Luttermoser & Johnson 1992), which complicates comparisons between cool giants stars. When comparing these fluxes of the Fe I (UV45) and C II] (UV0.01) emission lines, it should be noted that the C II] integrated flux as compared to the Mg II integrated flux is greater in carbon stars than it is in oxygen-rich cool giants (see Fig. 4 of Judge 1989). The observation that the Fe I (UV45) to C II] flux ratio is so much larger in the oxygen-rich Mira (e.g., R Hya) than in the carbon-rich SRb variable (e.g., TX Psc) suggests that the circumstellar envelope around oxygen-rich Mira variables may be significantly thicker than the carbon-rich non-Mira red giants. Mass-loss rates based on the CO (1–0) and/or (2–1) transitions give 9.1×10^{-8} $M_\odot$ yr^{-1} for TX Psc (Olofsson et al. 1993) and 4.0×10^{-7} $M_\odot$ yr^{-1} for R Hya (Hinkle et al. 1997)—over 4 times larger than the rate for TX Psc. It should be noted here that large systematic differences in derived mass-loss rates by various investigators have been noted in the past (Judge & Stencel 1991; Jorissen & Knapp 1998). The cause for these systematic differences lies in the adopted CO abundance ratio assumed by these investigators.

Opacities of C-rich and O-rich dust are quite different at optical and infrared wavelengths that have a significant effect on the emergent spectra of stars with circumstellar envelopes (see Fig. 3 of Wallerstein & Knapp 1998). The flux detected in the *IRAS* photometry bands (i.e., 12, 25, 60, and 100 μm) is dominated by emission from the circumstel-

TABLE 3

Hubble Space Telescope HRS INTEGRATED FLUXES OF EMISSION LINES[a]

Star (Phase)	Spectral Class	Observation Date	$F(K)$[b]	F(Mg II)/$F(K)$[c]	$F(k)/F(h)$	F(C II])/$F(K)$[c]	F(Fe I)/F(C II])[d]
μ Gem	M3 III	1993 Sep 27	10.9	117	1.65	5.84	0.0
R Hya (0.26).....	M7 IIIe	1996 Jul 9	19.1	65.5	0.43	0.038	6.1
R Leo (0.12)	M8 IIIe	1997 Jan 14	19.5	0.020	2.21	...	...
TX Psc.....	N0 II	1994 Dec 4	3.85	2.62	0.94	1.28	0.2
UU Aur	N3 II	1993 Nov 11	3.35	2.42	0.78	...	...

[a] Line fluxes are normalized to the K-magnitude flux.
[b] The integrated flux across the K band in units of 10^{-7} ergs s^{-1} cm^{-2}. The average of K_{max} and K_{min} are used for the Mira variables.
[c] Each number in the Mg II h and k and C II] normalized line fluxes should be multiplied by 10^{-7}.
[d] This Fe I flux is the (UV45) line at 2807.0 Å.

TABLE 4

Hubble Space Telescope HRS FWHM and Velocity Shifts of Emission Lines

	C II] (UV0.01)[a]		Fe I (UV44)		Fe I (UV45)	
Star (Phase)	FWHM[b]	RV[c]	FWHM	RV	FWHM	RV
μ Gem	0.26	−1.7	0.25	−1.9	...	...
R Hya (0.26).....	0.19	−10.1	0.33	−6.2	0.42	−12.1
R Leo (0.12)	...	...	...	...	...	...
TX Psc.....	0.32	−6.0	0.28	−8.7	0.30	−5.8
UU Aur	...	...	0.30	−12.0	0.21	−5.1

[a] Note that measured values for the lines in the C II] multiplet are averaged for those lines in the multiplet that have a signal-to-noise ratio of at least 2 and that are not compromised by circumstellar absorption.

[b] FWHM values are measured in Å, with uncertainties of ± 0.03 Å for each reported value.

[c] Radial velocity shifts (RV) are measured in km s^{-1}, with negative values indicating observed blueshifts, and correspond to gas outflowing away from the star. Velocity uncertainties with respect to the center-of-mass velocity are ± 0.7 km s^{-1} for each measurement.

lar shell in AGB stars (see Young, Phillips, & Knapp 1993). Much can be ascertained about the evolutionary state of cool stars by noting the location of such a star on an *IRAS* two-color diagram (e.g., van der Veen & Habing 1988). TX Psc falls in region VIa on the [25]−[60] versus [12]−[25] plot, which corresponds with objects that are mainly nonvariable, cool carbon stars with very cold dust at large distances from the star, though 24% of the stars in this group in the data set of van der Veen & Habing (1988) are variable. Meanwhile, R Hya lies in region II close to the region VII border in the two-color diagram. The majority of stars in region II are identified as (Mira) variable stars with relatively young oxygen-rich circumstellar shells.

For a given mass-loss rate, mass-losing time interval and similar photospheric effective temperatures, carbon stars are more obscured than oxygen stars for $\lambda < 2$ μm but are brighter than oxygen stars for $\lambda > 30$ μm, with the flux in the K band (2.2 μm) being relatively unaffected by the C/O ratio (see Fig. 3 of Wallerstein & Knapp 1998). The integrated flux comparisons between oxygen and carbon stars in the *IRAS* 12 and 25 μm bands is not trivial because of silicate emission bands seen in oxygen-rich shells. With these uncertainties in mind, an attempt to estimate the relative thickness of the circumstellar shells is now made assuming the shells of R Hya and TX Psc are of similar temperature. This is done to determine the validity of the analysis of the respective circumstellar shell thickness from the UV data. *IRAS* fluxes, normalized by the photospheric K-band flux, will be used for this comparison. The *IRAS* data are obtained from Loup et al. (1993) as shown in Table 5. The *IRAS* flux S is converted from janskys (Jy) to an integrated flux F in ergs s^{-1} cm^2 following equation (A.1a) from Loup et al. (1993). The K magnitudes of μ Gem, TX Psc, and UU Aur are −1.89, −0.76, and −0.61, respectively (Bergeat & Lunel 1980), and for the Mira variables R Hya and R Leo, the average K magnitudes of −2.50 and −2.52, respectively, will be used (Feast 1996; van Leeuwen et al. 1997). K magnitudes are then converted to integrated fluxes (ergs s^{-1} cm^2) using equation (2.28) of Henden & Kaitchuck (1982) in cgs units with a K-bandpass of 4800 Å. The results of these calculations are shown in Table 3 and used in both Tables 3 and 5. Note that in the three *IRAS* bands investigated, R Hya shows a much greater circumstellar flux than TX Psc—a factor of 19 times the brightness of TX Psc in the 12 μm band, 28 times in the 25 μm band, and 15 times in the 60 μm band. Hence, with the assumptions that have been outlined above, the infrared signatures of the circumstellar shells of these stars are consistent with the analysis of the Fe I (UV45) fluorescence above—R Hya appears to have a thicker circumstellar shell than TX Psc.

The strength (in terms of FWHM) of the fluoresced Fe I (UV44) (pumped by Mg II) is similar in all of the stars in our sample. However, the C II] lines are wider in the carbon AGB star (e.g., TX Psc) than in the noncarbon AGB stars (e.g., R Hya). Indeed, these lines may not be *optically thin* in the carbon stars (see Carpenter et al. 1997; Carpenter, Robinson, & Johnson 1998), no doubt because of the larger carbon abundances in these stars. However, the fluoresced Fe I (UV45) line is wider in the Mira star as compared with the carbon stars. Remember, this line is pumped by the C II] line at 2325.4 Å. Indeed, this is further proof that the circumstellar shell around Mira variables are substantially thicker than the non-Mira carbon stars, even though both stellar types show the circumstellar absorption over the Mg II lines.

As a prelude to carrying out NLTE radiative transfer calculations of hydrodynamic models of these stars, we follow the *approximate* technique described by Eriksson et al. (1986) of fitting the Mg II features with a series of Gaussians. Table 6 tabulates the results of this fitting for our Mira R Hya, and two non-Mira carbon stars, TX Psc and UU Aur. In this table, the radial velocity of the features are

TABLE 5

Infrared Flux Measurements[a]

Star	S_{12}	F_{12}	S_{25}	F_{25}	S_{60}	F_{60}	F_{12}/F_K	F_{25}/F_K	F_{60}/F_K	F_{12}/F_{25}	F_{12}/F_{60}
R Hya	1590	219	586	30.9	90.1	2.21	1.16	0.164	1.18×10^{-2}	7.09	99.1
TX Psc.....	163	22.4	39.8	2.10	11.9	0.292	6.15×10^{-2}	5.77×10^{-3}	8.02×10^{-4}	10.7	76.7

[a] The S fluxes are in units of jansky and the F fluxes are in units of 10^{-9} ergs s^{-1} cm^{-2}.

TABLE 6

GAUSSIAN PROFILE FITTING OF THE MG II LINES

Star (Phase)	R Hya (0.26)	TX Psc	UU Aur
Mg II Emission Gaussians			
RV[a]	−44	−15	−44
FWHM[b] (*k*, *h*)	(1.1, 0.8)	(1.1, 0.95)	(1.4, 1.1)
PEAK[c] (*k*, *h*)	(180, 155)	(2.0, 1.5)	(1.3, 1.1)
Mg II Self-Absorption Gaussians			
RV	+3.7	−17	−12
FWHM (*k*, *h*)	(0.80, 0.42)	(0.65, 0.30)	(0.75, 0.65)
Strong Circumstellar-Absorption Gaussians			
RV [Mn I (UV1)[d]]	−1.8	−14	−7.2
FWHM	0.50	0.40	0.60
RV [Fe I (UV3)[e]]	−6.0	−6.2	−11
FWHM	0.30	0.35	0.65
RV [Ti I (UV24)[f]]	−7.0	−3.6	−18
FWHM	0.30	0.30	0.70
RV [Fe I (UV3)[g]]	−7.4	−5.1	−2.0
FWHM	0.55	0.40	0.28

[a] Radial velocity at stellar rest frame in km s^{-1}; negative values indicate outflow. See text for a discussion of the velocity uncertainty of these measurements.

[b] FWHM for fitted Gaussian in Å. Uncertainty in the FWHM measurement is ±0.03 Å for each reported value.

[c] Peak flux of the fitted Gaussian in 10^{-13} ergs s^{-1} cm^2 $Å^{-1}$.

[d] Rest wavelength at 2794.817 Å.

[e] Rest wavelength at 2795.006 Å.

[f] Rest wavelength at 2802.465 Å.

[g] Rest wavelength at 2803.169 Å.

displayed with respect to the stellar rest frame for the various features. Figure 11 shows the resulting fit for R Hya. In this fitting technique, a Gaussian emission profile is fitted to the wings of the Mg II emission, velocity shifts are kept consistent for both the *k* and *h* lines and the ratio of the integrated flux of these profiles is constrained to match the ratio of respective oscillator strengths (e.g., ∼1.5) of these lines. The peak flux and the FWHM of these emission profiles are listed in Table 6 for each star. Note that the HRS instrument profile has *not* been deconvolved from the stellar profile in these measurements. The first thing to note is the relatively large velocity that the emission portion of Mg II has with respect to the photosphere of the stars. The sound speed in the outer atmospheres of these stars is typically around 10 km s^{-1}—the Mg II emission velocity is clearly supersonic in R Hya and UU Aur. Although the velocity for TX Psc's emission is somewhat lower than that of the other two stars, it should be noted that the *IUE* profile analyzed by Eriksson et al. (1986) gave an emission shift of −40 km s^{-1} for Mg II, similar to R Hya and UU Aur in our measurements. We next add an absorption Gaussian profile into the emission profile to represent the self-absorption of Mg II higher in the atmosphere. This self-absorption results from the decrease of opacity of the line as one travels higher in the atmosphere as the source function of the line decreases (see Luttermoser et al. 1989). Here is where the Mira star is fundamentally different from the non-Mira carbon stars. In the carbon stars, the self-absorption shows an outflow from the stars, whereas the Mira star shows a relatively stationary self-absorption. Qualitatively, such a macroscopic velocity shift for the Mira is consistent with the velocity field of hydrodynamic models of Mira variables (e.g., Bowen 1988; Fleischer et al. 1992), that is, the gas velocity in the shock is larger than the gas velocity in the outermost region of the atmospheric model. From the emission of Mg II, the atmospheres of the Mira variables and non-Mira carbon stars must have shocks propagating through them. However, the velocity profiles are not the same higher in the atmosphere. In summary, the atmospheric structure difference between semiregular variable carbon stars and oxygen-rich Mira variables is more of a quantitative than qualitative nature, which also was pointed out by Hinkle et al. (1997)—the physics governing the two types of stars (and especially the presence of a shock) is probably very similar.

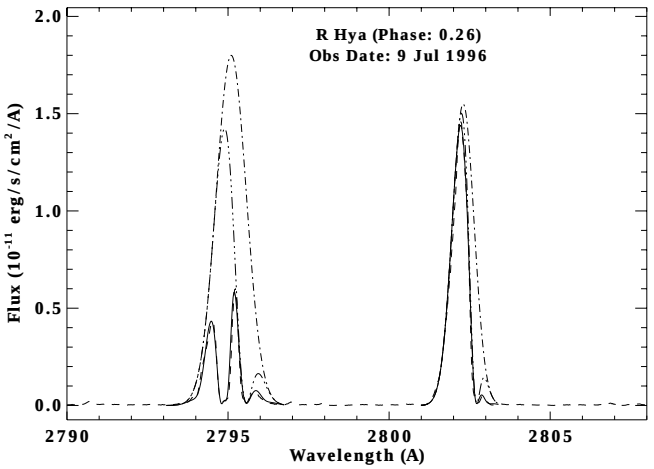

FIG. 11.—Gaussian emission profiles (*dot-dashed line*) with overlying Gaussian self-absorption profiles (*triple-dot–dashed line*) and circumstellar absorption give a final profile (*solid line*) that gives the best fit to the observed Mg II features (*dashed line*) of R Hya. The Gaussian profile parameters for these profiles are listed in Table 6.

As stated earlier, the Mg II doublet also shows evidence of overlying absorption from neutral metal lines arising from a cooler circumstellar shell around the star. Table 6 shows the results of the fits of the four main lines that contribute to the asymmetries seen in Mg II *h* and *k*. A majority of these lines show a low expansion velocity. Since the overlying obscuration is so extreme in these stars, we did not try to add an interstellar absorption profile from Mg II. This, of course, increases the uncertainty in the placement of the circumstellar absorbers, unless the interstellar medium feature is coincident with the atmospheric self-absorption of Mg II. Also note that additional overlying lines were sometimes needed to get an *exact* fit to the observed profiles: Fe I (UV124) at 2794.157 Å, Zr I (UV4) at 2795.140 Å, and Fe I (UV44) at 2795.540 Å. All of the circumstellar transitions were selected based on the criterion that they be neutral metals with a lower energy levels less than 3 eV.

The above analysis is only approximate at best. In reality, Mg II forms over a large region in the outer atmospheres of these stars where the macroscopic velocity is continually changing with height (and time). As such, a *two-component* fit to these lines can lead to unanticipated errors in the velocity measurements. Instead, NLTE radiative transfer modeling must be performed to confirm our approximate measurements. Finally, since one has many *free parameters* to play with when performing Gaussian fits, uncertainties also arise in the placement of the Gaussians. It was found from this analysis that the uncertainties in the velocities of

all our fits are on the order of 5–10 km s^{-1}. The Gaussian *emission* profile uncertainty is large when overlying absorption lies near the edges of the Mg II line wings.

5. CONCLUSION

We have obtained high-resolution UV spectra of two Mira stars, R Hya and R Leo. The spectrum of R Leo was obtained at phase 0.12, which presented very weak Mg II lines and nothing else. Given the low signal-to-noise ratio, we were unable to carry out any analysis with this spectrum. The R Hya spectrum, taken at phase 0.26, shows a remarkable amount of detail that has enabled us to carry out a preliminary analysis. The following results were found from this analysis.

1. A new fluoresced emission line was discovered for oxygen-rich stars—the Fe I (UV45) line near 2807 Å, which is pumped by the strongest line of the C II] (UV0.01) line at 2325.5 Å. Prior to this observation, this fluorescence had been seen only in cool carbon stars.

2. Velocity shifts of emission features in the UV spectra of Mira variables are consistent with previously published hydrodynamic models of these stars.

3. Velocity measurements indicate that the C II] (UV0.01) emission lines are not formed in the same atmospheric layers as the Mg II emission. The exact location of the formation depths of these lines must await the results of NLTE modeling.

4. The electron density deduced from the C II] (UV0.01) multiplet is $\sim 10^9$ cm^{-3}.

5. The temperature-density structure of the semiregular variable carbon stars is similar to the oxygen-rich Mira variables—both are hydrodynamic in nature; however, the carbon star macroscopic velocity field is not identical to the Mira star in the atmosphere layers between the Mg II emission region and the circumstellar shell.

These findings suggest that the non-Mira carbon stars are pulsating just as is the case for the Mira stars, where this pulsation gives rise to outward moving shocks in their atmospheres. This statement is based on the velocity shifts and line profiles seen in the emission lines of their UV spectra. High-resolution UV observations like these, used in conjunction with hydrodynamic and NLTE radiative transfer modeling, will lead to a more complete understanding of the outer layers of these stars. A monitoring program for a set of Mira variables and semiregular variables at high dispersion (perhaps with STIS) over a few pulsation cycles would be invaluable in understanding the details of the structure of these important stars.

Support for this work was provided by NASA through grant number GO-06620.01-95A from the Space Telescope Science Institute, which is operated by the Association of Universities for Research in Astronomy, Inc., under NASA contract NAS 5-26555. I am grateful for this support. As well, I wish to thank East Tennessee State University undergraduate student Ms. Susan Mahar who helped in the data analysis of this research. Analysis of the *IUE* and McMath-Pierce data was supported under NASA grant NAG 5-1777 to Iowa State University. I am grateful to the observing assistance from the staff at the *IUE* Observatory at NASA/Goddard Space Flight Center and for the ground-based support from Ms. Trudy Tillman (NSO Synoptic Observer) and Mr. Dave Jaksha (NSO technical support). Useful conversations with Drs. L. A. Willson and G. H. Bowen about Mira variables are appreciated as well. Finally, I wish to thank M. W. Castelaz for useful comments on this manuscript. For information on related research, please see http://www.etsu.edu/physics on the World Wide Web.

REFERENCES

Barnbaum, C. 1992, ApJ, 385, 694
Bergeat, J., & Lunel, M. 1980, A&A, 87, 139
Bessell, M. S., Scholz, M., & Wood, P. R. 1996, A&A, 307, 481
Bidelman, W. P., & Herbig, G. H. 1958, PASP, 70, 451
Bookbinder, J. A., Brugel, E. W., & Brown, A. 1989, ApJ, 342, 516
Bowen, G. H. 1988, ApJ, 329, 299
Brugel, E. W., Beach, T. E., Willson, L. A., & Bowen, G. H. 1987, in IAU Colloq. 103, The Symbiotic Phenomena, ed. M. Friedjung (Dordrecht: Reidel), 67
Carpenter, K. G., Robinson, R. D., & Johnson, H. R. 1998, in ASP Conf. Proc. 154, Cool Stars, Stellar Systems, and the Sun, 10th Cambridge Workshop, ed. R. Donahue & J. A. Bookbinder (San Francisco: ASP), 1578
Carpenter, K. G., Robinson, R. D., Johnson, H. R., Eriksson, K., Gustafsson, B., Pijpers, F. P., Querci, F., & Querci, M. 1997, ApJ, 486, 457
Carpenter, K. G., Robinson, R. D., & Judge, P. G. 1995, ApJ, 444, 424
Carpenter, K. G., Wing, R. F., & Stencel, R. E. 1985, ApJS, 57, 405
Di Benedetto, G. P., & Conti, G. 1983, ApJ, 268, 309
Drinkwater, M. J., & Wood, P. R. 1985, in Mass Loss from Red Giants, ed. M. Morris & B. Zuckerman (Dordrecht: Reidel), 257
Eriksson, K., Gustafsson, B., Johnson, H. R., Querci, F., Querci, M., Baumert, J. H., Carlsson, M., & Olofsson, H. 1986, A&A, 161, 305
Feast, M. W. 1996, MNRAS, 278, 11
Fleischer, A. J., Gauger, A., & Sedlmayr, E. 1992, A&A, 266, 321
Gillet, D. 1988, A&A, 192, 206
Haniff, C. A., Scholz, M., & Tuthill, P. G. 1995, MNRAS, 276, 640
Henden, A. A., & Kaitchuck, R. H. 1982, Astronomical Photometry (New York: Van Nostrand Reinhold)
Hinkle, K. H., Lebzelter, T., & Scharlach, W. W. G. 1997, AJ, 114, 2686
Hinkle, K. H., Scharlach, W. W. G., & Hall, D. N. B. 1984, ApJS, 56, 1
Hoefner, S., & Dorfi, E. A. 1997, A&A, 319, 648
Johnson, H. R. 1987, in Cool Stars, Stellar Systems, and the Sun, 5th Cambridge Workshop, ed. J. L. Linsky & R. E. Stencel (Berlin: Springer), 399
Johnson, H. R., Ensman, L. M., Alexander, D. R., Avrett, E. H., Brown, A., Carpenter, K. G., Eriksson, K., Gustafsson, B., Jørgensen, U. G., Judge, P. D., Linsky, J. L., Luttermoser, D. G., Querci, F., Querci, M., Robinson, R. D., & Wing, R. F. 1995, ApJ, 443, 281
Jørgensen, U. G. 1989, ApJ, 344, 901
Jorissen, A., & Knapp, G. R. 1998, A&AS, 129, 363
Judge, P. G. 1989, in IAU Colloq. 106, Evolution of Peculiar Red Giant Stars, ed. H. R. Johnson & B. Zuckerman (Cambridge: Cambridge Univ. Press), 303
Judge, P. G., Luttermoser, D. G., Neff, D. H., Cuntz, M., & Stencel, R. E. 1993, AJ, 105, 1973
Judge, P. G., & Stencel, R. E. 1991, ApJ, 371, 357
Leitherer, C. 1995, *HST* Data Handbook, vol. 2 (Baltimore: STScI)
Lennon, D. J., Dufton, P. L., Hibbert, A., & Kingston , A. E. 1985, ApJ, 294, 200
Little, S. J., Little-Marenin, I. R., & Bauer, W. H. 1987, AJ, 94, 981
Loup, C., Forveille, T., Omont, A., & Paul, J. F. 1993, A&AS, 99, 291
Luttermoser, D. G. 1996, in ASP Conf. Proc. 109, Cool Stars, Stellar Systems, and the Sun, 9th Cambridge Workshop, ed. R. Pallavicini & A. K. Dupree (San Francisco: ASP), 535
———. 1999, in IAU Symp. 177, The Carbon Star Phenomenon, ed. R. F. Wing (Dordrecht: Kluwer), in press
Luttermoser, D. G., & Bowen, G. H. 1990, in ASP Conf. Proc. 9, Cool Stars, Stellar Systems, and the Sun, 6th Cambridge Workshop, ed. G. Wallerstein (San Francisco: ASP), 491
———. 1992, in ASP Conf. Proc. 26, Cool Stars, Stellar Systems, and the Sun, 7th Cambridge Workshop, ed. M. S. Giampapa & J. A. Bookbinder (San Francisco: ASP), 558
Luttermoser, D. G., & Johnson, H. R. 1992, ApJ, 388, 579
Luttermoser, D. G., Johnson, H. R., Avrett, E. H., & Loeser, R. 1989, ApJ, 345, 543
Merrill, P. W. 1940, Spectra of Long-Period Variable Stars (Chicago: Univ. of Chicago Press)
Moore, C. E. 1950, NBS Circ., No. 488

Olofsson, H., Eriksson, K., Gustafsson, B., & Carlström, U. 1993, A&AS, 87, 267
Quirrenbach, A., Mozurkewich, D., Hummel, D. F., Buscher, D. F., & Armstrong, J. T. 1994, A&A, 285, 541
Stencel, R. E., Linsky, J. L., Brown, A., Jordan, C., Carpenter, K. G., Wing, R. F., & Czyzak, S. 1981, MNRAS, 196, 47P
Udry, S., Jorissen, A., Mayor, M., & Van Eck, S. 1998, A&AS, 131, 25
van der Veen, W. E. C. J., & Habing, H. J. 1988, A&A, 194, 125
van Leeuwen, F., Feast, M. W., Whitelock, P. A., & Yudin, B. 1997, MNRAS, 287, 955
Wallerstein, G., & Knapp, G. R. 1998, ARA&A, 36, 369
Willson, L. A. 1976, ApJ, 205, 172
Willson, L. A., Wallerstein, G., & Pilachowski, C. A. 1982, MNRAS, 198, 483
Wilson, R. E. 1953, Gen. Cat. of Stellar Radial Velocities, Carnegie Inst. Washington Publ. 601
Wood, P. R. 1975, MNRAS, 171, 15P
Young, K. 1995, ApJ, 445, 872
Young, K., Phillips, T. G., & Knapp, G. R. 1993, ApJ, 409, 725
Zuckerman, B., & Dyck, H. M. 1986, ApJ, 304, 394